Structure and tribological properties of Si/a-C:H(Ag) multilayer film in stimulated body fluid*

Yan-Xia Wu(吴艳霞)[1], Yun-Lin Liu(刘云琳)[1], Ying Liu(刘颖)[1], Bing Zhou(周兵)[1], Hong-Jun Hei(黑鸿君)[1], Yong Ma(马永)[1], Sheng-Wang Yu(于盛旺)[1,†], and Yu-Cheng Wu(吴玉程)[1,2,‡]

[1] *Institute of New Carbon Materials, Taiyuan University of Technology, Taiyuan* 030024, *China*
[2] *Key Laboratory of Interface Science and Engineering in Advanced Materials (Taiyuan University of Technology), Ministry of Education, Taiyuan* 030024, *China*

(Received 21 April 2020; revised manuscript received 25 May 2020; accepted manuscript online 12 June 2020)

Si/a-C:H(Ag) multilayer films with different modulation periods are prepared to test their potential applications in human body. The composition, microstructure, mechanical and tribological properties in the simulated body fluid are investigated. The results show the concentration of Ag first decreases and then increases with the modulation period decreasing from 984 nm to 250 nm. Whereas the C content has an opposite variation trend. Notably, the concentration of Ag plays a more important role than the modulation period in the properties of the multilayer film. The a-C:H sublayer of the film with an appropriate Ag concentration (8.97 at.%) (modulation period of 512 nm) maintains the highest sp^3/sp^2 ratio, surface roughness and hardness, and excellent tribological property in the stimulated body fluid. An appropriate number of Ag atoms and size of Ag atom allow the Ag atoms to easily enter into the contact interface for load bearing and lubricating. This work proves that the Ag nanoparticles in the a-C:H sublayer plays a more important role in the tribological properties of the composite-multilayer film in stimulated body fluid condition.

Keywords: Si/a-C:H(Ag) multilayer film, modulation periods, Ag concentration, tribological properties

PACS: 61.05.–a, 68.37.–d **DOI:** 10.1088/1674-1056/ab9c10

1. Introduction

Hydrogenated amorphous carbon (a-C:H) films possess advantages of high hardness, chemical inert, low friction and wear, and anti-corrosion, implying great potential applications in many fields, such as biomedicine, ocean, and space.[1,2] However, the high internal stress and low adhesive strength limit the practical applications of the film.[3] What is even worse is that the tribological properties of the film are environment-sensitive. It shows that there exist high friction and wear in liquid and oxygen environment. This can be solved by designing composites or multilayer films.[4,5] For example, Ag nanoparticles, each with a face-centered cubic structure and small elastic modulus than the a-C:H, incorporated into a-C:H film demonstrates that it is a promising candidate for the protective layers due to its low internal stress, hemo-compatibility, antibacterial properties, low friction coefficient, and wear rate in both air and vacuum.[6–9] Inevitably, this film usually still has relatively low hardness, which limits its practical applications.[10]

Multilayer structure is alternative design to improve the mechanical and tribological properties of a-C:H film. The film combined with the soft layer can provide low friction and hard layer to achieve bearing capacity. The interface between different sublayers can effectively prevent the crack and absorb dislocation from growing. As reported before, the Si/a-C:H multilayer film with moderate modulation period exhibits high hardness, low friction, and wear in liquid lubrication.[11] The micro-scaled a-Si/C multilayer thin films (1.1 μm) used as anode materials for lithium ion batteries also showed a good cycling performance.[12,13] Based on the Si atom able to bond with C atom and thus forming SiC at the interface, it can also increase the hardness of the multilayer film. This shed light on the method to synthesize films that have combined advantages of each sublayer without changing the properties of them.

Bearing these in mind, the combination of the composite and multilayer structure may reduce the internal stress and improve the tribological properties of the a-C:H film in liquid environment without degrading its harness. However, researches on this method are rare indeed. The few researches have proved that the combined structure owns excellent properties,[14,15] for example, the alternating multilayer diamond-like carbon (DLC) films [(Cr, N)-DLC/DLC] shows low internal stress, high toughness, good adhesion.[16] Therefore, it is necessary to investigate such a structure further.

Here in this work, a-C:H(Ag) composite sublayer and Si sublayer deposited by magnetron sputtering technique, are

*Project supported by the National Natural Science Foundation of China (Grant Nos. 51801133, 51505318, and 51671140), the Science and Technology Major Project of Shanxi Province, China (Grant No. 20181102013), the Shanxi Provincial Youth Fund, China (Grant No. 201801D221135), and the "1331 Project" Engineering Research Center of Shanxi Province, China (Grant No. PT201801).

†Corresponding author. E-mail: yushengwang@tyut.edu.cn
‡Corresponding author. E-mail: wyc@tyut.edu.cn

© 2020 Chinese Physical Society and IOP Publishing Ltd

combined together to achieve high hardness, low friction, and wear in biological environment. The influences of different modulation periods on composition, structure, mechanical and tribological properties of the film are discussed.

2. Experimental details

2.1. Film deposition

Si/a-C:H(Ag) multilayer films with different modulation periods were deposited on silicon wafers and stainless-steel substrates by magnetron sputtering. Two circular targets (Φ50.3 mm×5 mm) consisting of Si and graphite/Ag were used alternatively during the deposition. The Si target was connected to a medium pulsed DC power supply operated at 80 W and 80% duty circle with sputtering gas of Ar (the gas flow rate was 62 sccm and the corresponding pressure was 0.7 Pa). While the graphite/Ag target was connected to an RF power supply operated at 150 W with Ar and CH_4 plasmas (the Ar gas flow rate was 40 sccm and the CH_4 gas flow was = 20 sccm, pressure = 0.7 Pa). The substrates were cleaned ultrasonically in an acetone bath and dried in air and then etched with Ar^+ ions in the vacuum chamber to remove the contamination from the surface. Consequently, different sublayers (Si and a-C:H(Ag)) were deposited alternatively on the substrate. To vary the modulation period of the film, the alternate deposition times of different films on each sublayer were 45 min, 30 min, 20 min, and 15 min, which are denoted as A1, A2, A3, and A4, respectively. The total deposition time was 3 h.

2.2. Microanalysis and testing methods

The chemical composition of the film was examined by x-ray photoelectron spectroscopy (XPS, ESCA-PHI 5500), with Al-$K\alpha$ radiation as the excitation source. The Au 4f at 84.7 eV was used to calibrate the binding energy of Ag (3d) and C (1s). Raman scattering spectroscopy with an excitation wavenumber of 532 nm was used to detect the carbon bonding. The functional structure was obtained by Fourier transform infrared spectroscopy (FTIR, Bio-RAD FTS 40). The surface and cross-sectional morphologies were obtained by atomic force microscope (AFM, MFT-R4000) and field emission scanning electron microscopy (FESEM, S-5500, with acceleration voltage of 10 kV), respectively. The crystallographic structures were obtained by glancing angle x-ray diffraction (XRD, Jobin-Yvon HR-800) spectra with Cu-$K\alpha$ radiation at the working power of 40 kV×40 mA.

The mechanical properties (hardness and elastic modulus) were evaluated by a nanoindentation (MZT-4, AKASHI Co.) and the maximum indentation depth was controlled to be about 100 nm (less than 10% of the film thickness) to minimize the effect of the substrate. The thickness and curvature of the film deposited on Si wafer were measured by a Micro XAM 3D non-contact surface profilometer (ADE shift, USA). The internal stress was evaluated by substrate curvature method and calculated from Stoney equation:

$$\sigma = \frac{E_s}{6(1-\nu_s)}\left(\frac{t_s^2}{t_f}\right)\left(\frac{1}{R_2}-\frac{1}{R_1}\right),$$

where σ is the internal stress, the ν_s and E_s are the Poission ratio and Young modulus of the silicon substrate, respectively, t_s and t_f are the thickness of the substrate and film, respectively, R_2 is the curvature of the film deposited on Si wafer. The curvature of the Si flat wafer (R_1) before deposition of the films is assumed to tend to be infinite. Young's modulus of 131 GPa and the Poisson ratio of 0.278 are adopted for Si p(111) substrate.

The tribological properties of the films were tested on the reciprocating ball-on-disk tribometer (MFT-R4000) in simulated body fluid with a 5-mm-diameter Al_2O_3 steel ball as counterpart, normal load of 2 N, sliding time of 30 min, oscillation frequency and amplitude of 2 Hz and 5 mm, respectively. The contact area was filled with simulated body fluid, which is composed of the following ingredients: 8.035-g/L NaCl, 0.355-g/L $NaHCO_3$, 0.225-g/L KCl, 0.231-g/L $K_2HPO_4{\cdot}3H_2O$, 0.311-g/L $MgCl_2{\cdot}6H_2O$, 1.0-M HCl (39 ml), 0.292-g/L $CaCl_2$, and 0.072-g/L Na_2SO_4 in deionized water and the pH was adjusted to 7.4 by adding 6.118-g/L trishydroxymethyl aminomethane (Tris) and 1.0-M HCl at 37 °C.[17] Friction experiments were conducted thrice under each experimental condition. The wear track on the film was observed by MicroXAM-3D surface profiler. The worn surfaces and the counterpart balls were observed by a scanning electron microscope (SEM), operated at an acceleration voltage of 20 kV and equipped with an energy dispersive spectrometer.

3. Results and discussion

3.1. Film composition and structure

The typical cross-sectional FESEM images of the multilayer films with different modulation periods are given in Fig. 1. It can be seen that the multilayer film shows a homogeneous and dense microstructure, without any obvious defects, or pores or pinholes on it. The modulation period decreases from 948 nm to 512 nm to 357 nm and to 250 nm) with the deposition time of each sublayer decreasing from 45 min to 30 min to 20 min and to 15 min. Meanwhile, the columnar crystal-like Si sublayer is a little thicker than the composite C:H(Ag) sublayer due to the higher sputtering yield. Especially, two sublayers with very small thickness difference in A3 may be attributed to the most serious poisoning of the target in this alternative deposition time. The absorbed CH_4 and related species ($CH_3{\cdot}$, H·, $CH_2{\cdot}$, CH·, *etc.*) can cause the coverages of both targets to increase during the deposition of the a-C:H(Ag) sublayer. Therefore, the sputtering yields of these

targets are initially low until the surface layer is removed. Here in this work, the thickness of Si decreases whereas the thickness of a-C:H increases. However, the thickness of the whole multilayer film, *i.e.*, the total thickness, is about 1.7 μm, indicating that the deposition time of sublayer has little effect on the total thickness of the film. The interface between the sublayers is combined well without any obvious defects.

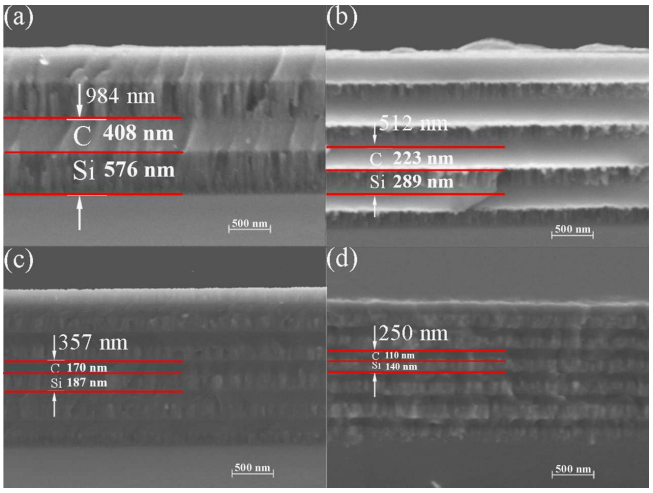


Fig. 1. Typical cross-sectional FESEM images of multilayer films with different modulation periods.

The effect of different modulation periods on the chemical composition of the multilayer film is analyzed by XPS, and the corresponding results are given in Table 1. It is noted that the C content increases to 82.33 at.% and then decreases to 80.93 at.%. The O content shows the same varying trend with C content, indicating that some O atoms may react with C atoms on the surface. The O atoms can derive from the surface adsorption. Whereas, Ag atoms show an opposite trend with modulus decreasing. Generally, the nanoparticle Ag in the composite film can hinder the film from oxidizing.

Table 1. Chemical compositions of multilayer films with different modulation periods.

Sample	Chemical composition/at.%		
	C content	Ag	O
A1	62.82	28.92	8.27
A2	82.21	8.97	8.82
A3	82.33	0.57	17.10
A4	80.93	10.01	9.06

Combining the XPS spectra of Ag 3d in Fig. 2, two characteristics peaks centered at 367.6 eV and 373.6 eV are assigned to Ag 3d5/2 and Ag 3d3/2, respectively. The difference between these peaks is 6.0 eV, inferring that Ag species incorporated into the films are in metallic form.[18] Additionally, the intensity of Ag in A3 sample is nearly zero, indicating less Ag content. The resulting composition of the film depends on sputter yield of the film. The sputter yield depends on the target element, the sputter gas, ion incident angle, sputtering time, *etc*. The sputter yield varies with sputter time. Especially for the film deposited with Ar and CH_4, which can cause the composite target to poisoning during the deposition. Therefore, the Ag content varies significantly with the modulation period. The most serious poison of the target causes the target element to produce the least sputtering yield and thus the least Ag content in the film.

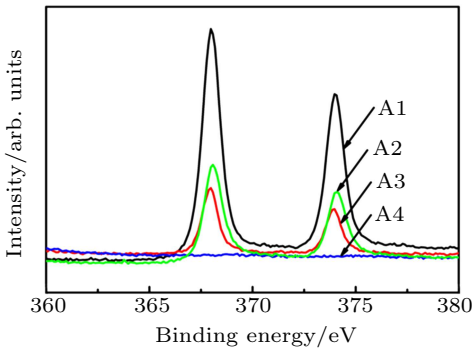


Fig. 2. XPS spectra of Ag 3d in multilayer film.

The C 1s peaks in Fig. 3 can be fitted with Gaussian distributions, and the peak centered at about 284.5, 285.3, 287.8, and 288.5 eV correspond to sp^2-hybridized C, sp^3-hybridized C, C=O, and O=C–OH bonds, respectively. The dominance of the distribution centered at ∼ 284 eV indicates that all films are rich in sp^2 C bonding. The high sp^2 C content can be explained by the fact as given below. First, the sputtering of the graphite target inclines to the forming of sp^2 C: incident ions on the film surface are decomposed by the low-energy CH_4 during the film growth, and are likely to form sp^2 C. Second, although none of Ag particles in the film bonds with C particles, many Ag particles aggregating large enough can interrupt the C network and induce the sp^2 C to form. Third, the sputtered particles with low energy are too weak to penetrate into the subsurface of the film, and then they tend to form more sp^2 C bonds.

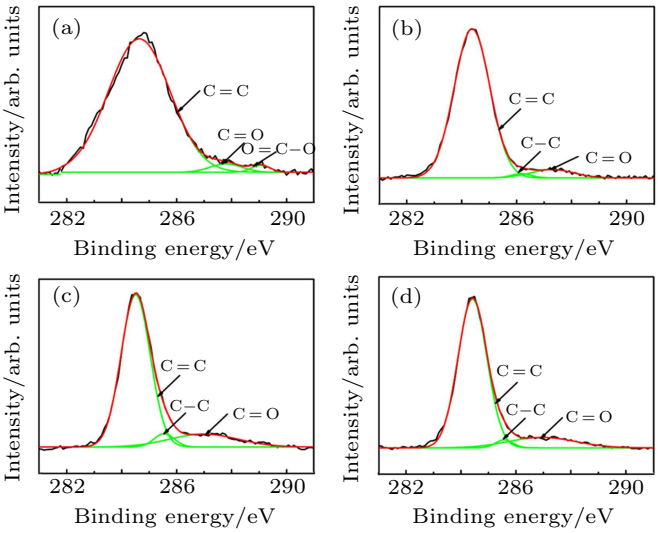


Fig. 3. XPS spectra of C 1s peaks in multilayer film fitted by deconvoluted peaks.

To further analyze the phase information about the multilayer film, the XRD pattern of the film with the highest and lowest C content, which are in accordance with that of A1 sample and A3 sample, are given in Fig. 4. The broad hump in the region 20°–26° can be assigned to the amorphous C sublayer.[19] All patterns present two peaks assigned to Ag. The relative intensity of Ag in the A3 is much lower than that in the A1 sample, demonstrating a reduced Ag content in the A3, which is confirmed by the XPS result. Additionally, other two peaks illustrate the existence of Si (320) and Si (331) planes, corresponding to the Si sublayer in the multilayer film. There is also a peak assigned to SiC (007) at 50.6°, indicating the formation of SiC at the interface of the sublayers. Obviously, the relative intensity between Si and SiC diffraction peak demonstrates an increase with modulation period decreasing, indicating that the volume fraction or crystallization of Si and SiC crystal increase.[20] Since the SiC forms at the interface of the sublayer in the film, the increased number of the interlayer in A3 as shown in Fig. 1 can cause the fraction of SiC to increase.

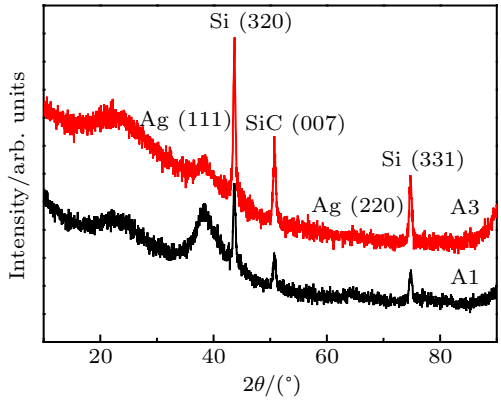


Fig. 4. XRD pattern of A1 (highest C content) and A3 (lowest C content) sample.

Raman spectra can give the carbon features of the a-C:H based film. Figure 5 shows the Raman spectra including deconvolution peaks, obtained from the Si/a-C:H(Ag) multilayer films. The G-peak centered at ~ 1590 cm^{-1} is due to in-plane stretching of sp^2-bonded C atoms existing in olefinic chains and aromatic rings, while the D-peak centered at ~ 1350 cm^{-1} is due to the breathing mode (out-of-plane stretching) of sp^2-bonded C atoms existing only in the aromatic rings. A third peak at 1470 cm^{-1} can be identified with semicircle stretching vibration of carbon atoms in benzene or benzene clusters,[21] indicating a high sp^2 C in the composite film, which is consistent with the XPS results. The relative intensity of D peak and G peak, corresponding to I_D/I_G ratio and G position, are widely used to identify the sp^3/sp^2 ratio amorphous carbon.[22] The increase in I_D/I_G ratio and G peak frequency indicate the decreasing of sp^3/sp^2 ratio and graphitization of the film.[22,23] As given in Table 2, the I_D/I_G ratio and the G peak position first decrease first and then increase. The A2 sample has the highest sp^3/sp^2 ratio. Whereas, the A1 sample has the lowest sp^3/sp^2 ratio. Combining XPS spectra, A1 sample contains the highest Ag concentration, Ag nanoparticles in the film induce sp^2 C to form. Although the A3 sample contains the least Ag nanoparticles in the sample, the O in the film may cause higher concentration of sp^2 C than in the A2 sample.

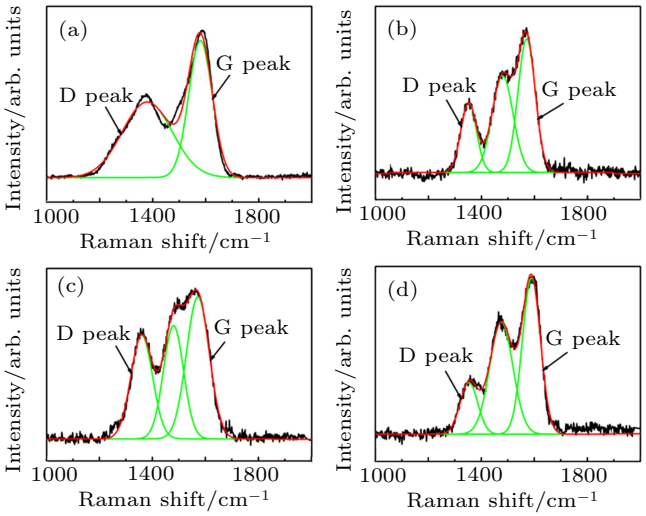


Fig. 5. Raman spectra, including deconvolution peaks, obtained from Si/a-C:H(Ag) multilayer films.

Table 2. I_D/I_G ratios and G peak positions of multilayer film.

Sample	A1	A2	A3	A4
G peak position/cm^{-1}	1596	1569	1571	1590
I_D/I_G ratio	2.21	0.73	1.07	1.26

The FTIR spectrum can be used for identifying the different vibrational modes in the a-C:H multilayer film. Figure 6 gives the FTIR information of the multilayer film. The absorption peak at 610 cm^{-1} is attributed to stretching vibration of C–C. The absorption peak at ~ 784 cm^{-1} is ascribed to the vibration of Si–C mode, indicating the formation of SiC at the interface of sublayers for each of all these multilayer films. The absorption peak at 875 cm^{-1} is assigned to C–O stretching bond and the peaks appearing at 1000 cm^{-1}–1100 cm^{-1} belong to the –C–O–C– groups.[24] The absorption peaks in a range from 2700 cm^{-1} to 3100 cm^{-1} are caused by C–H stretching in CH, CH$_2$, and CH$_3$ groups,[25] indicating H mainly bonded with sp^3 C in the film. The two peaks located at 2877 cm^{-1} and 2958 cm^{-1} are corresponding to the symmetric stretching vibration of sp^3 CH$_3$, and the peak located at 2922 cm^{-1} is assigned to the symmetric stretching vibration of sp^3 CH$_2$. It is no doubt that the hydrogen atom is mainly bonded with sp^3 C in the films.

The AFM images of an area of 3 μm ×3 μm of the multilayer films with different modulation periods are shown in

Fig. 7. There are little differences in surface roughness among these films. They are mainly composed of small spheres with some acicular-like particles on it. The surface roughness of the film can be a combined result of modulation period, sp^3 C and Ag nanoparticles content on the surface. Generally, high sp^3 C, low Ag content and small modulation period conduce to forming the low surface roughness of the film.[26,27]

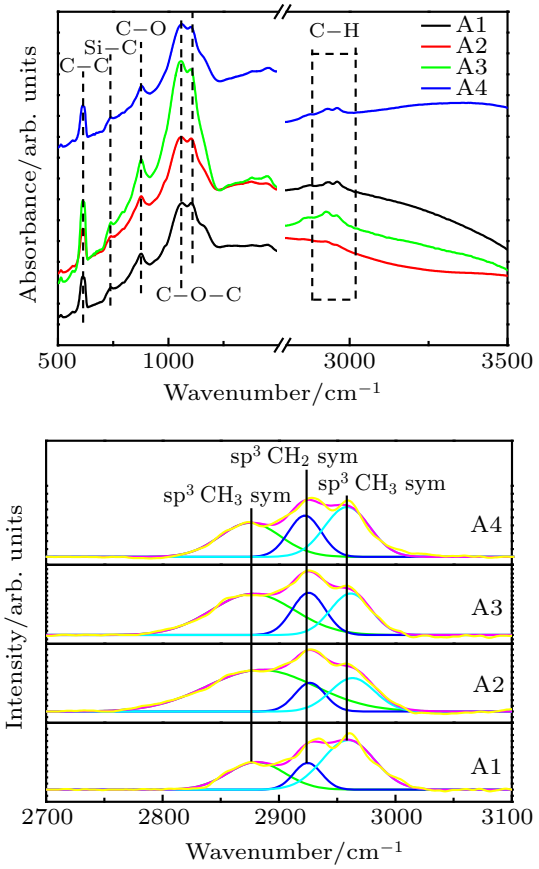


Fig. 6. (a) Curves for FTIR information of multilayer film and (b) their partial amplification.

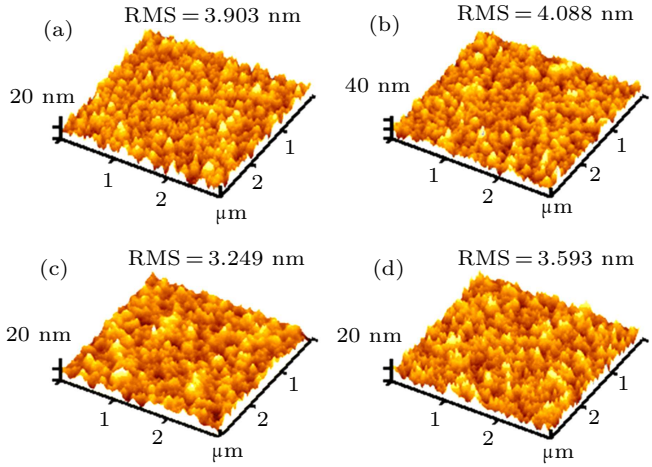


Fig. 7. AFM images of 3 μm × 3 μm area of multilayer films.

3.2. Mechanical properties

Figure 8 shows the values of hardness and elastic modulus of the multilayer films. A2 sample shows the highest hardness. The modulation periods, Ag nanoparticle and sp^3 C content play an important role in the hardness. The dense interfaces between the sublayers can contribute to the high hardness. More interfaces in the multilayered films act as energy dissipating and crack propagation reducing sites, and thus improving the mechanical properties of the film.[28] It was reported that when the nanocrystalline/amorphous system has an appropriate size of crystalline grains dispersed and separated by 1 nm–3 nm amorphous matrix, the hardness of such a system will be elevated by restricting the dislocation operation and crack propagation.[29] However, high nanoparticle content would aggregate and degrade the connectivity of the carbon network, cause low hardness consequently. Therefore, the high hardness of A2 and A4 samples can be attributed to the appropriate Ag content. While too few or too many Ag atoms in the film can weaken the hardness of the film. A large number of interfaces parallel to the substrate surface have a hardening effect in the multilayer film.[30] Furthermore, the highest sp^3 C content in A2 sample can increase the rigidity and improve the connectivity of the amorphous carbon network, hence increase the hardness of the film. The lowest hardness of the A3 sample can be attributed to the oxidation of the film because of the highest O content as given in the XPS spectra. The sufficient O atoms on the surface can combine with C atoms, causing terrible oxidation and reduce the connectivity and rigidity of the C network, and thus the film shows the lowest hardness.

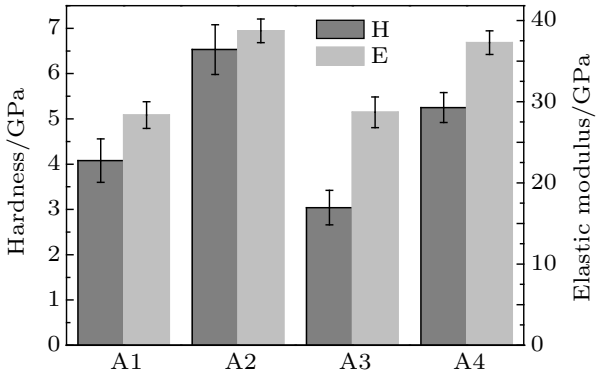


Fig. 8. Hardness and elastic modulus of multilayer films.

The calculated internal stress values corresponding to A1, A2, A3, and A4 sample are 0.79, 0.37, 0.23, and 0.15 GPa, respectively. All the multilayer films maintain relatively low internal stress. The decreasing of internal stress in the film can be attributed to the increase of the number of the sublayers in the film. Because different multiple sublayers of alternating deposition can neutralize internal stress, and more interface in the film can effectively prevent the micro-crack and dislocation slip from being pregnant and growing, The resulting film can have a lower internal stress.

3.3. Tribological properties

Figure 9 presents the frictional curves of the multilayer films measured by the tribometer on the reciprocating ball-on-disk tribometer in simulated body fluid against Al_2O_3 steel ball at room temperature. As shown in Fig. 9, A3 sample possesses the most fluctuating and highest friction coefficient in a range of $\sim$ 0.09–0.23. This relatively large fluctuation in friction coefficient indicates the extensive surface damage (wear) and the entrapment of a greater number of wear debris at the sliding interface. A1 sample shows higher friction coefficient in a longer running-in period, indicating a severe wear at first. Whereas, A2 and A4 samples show steady friction coefficient of about 0.1 during the test.

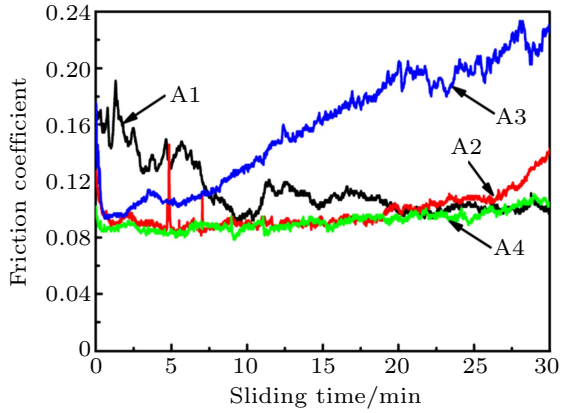


Fig. 9. Frictional curves of multilayer films, measured by tribometer on reciprocating ball-on-disk tribometer in simulated body fluid against Al_2O_3 steel ball at room temperature.

In order to gain more insights into the friction and wear mechanism, the three-dimensional (3D) optical profile images of the worn film surfaces and the SEM images of corresponding Al_2O_3 ball surface are shown in Figs. 10 and 11, respectively. Although the friction test is performed in the simulated body liquid, there is no obvious sign of corrosion on the counterpart except for A1 sample. This can be confirmed by the high and fluctuant friction coefficient (Fig. 9) and relatively high wear of A1 (Fig. 10). The wear track of the A2 sample is the shallowest with some plows on it, indicating the lowest wear volume and wear rate. The transfer film on its counterpart is dense with a few aggregate wear debris on it, which can irritate the plow on the film. In contrast, the wear track of A3 is the widest and deepest, indicating the highest wear volume and wear rate. The transfer film on the counterpart ball consists of some bumps aggregated by wear debris, and even peel-off debris. These imply an intensive wear and high friction during the friction test. The friction and wear of the A1 and A4 are medium. Comparatively, the wear of A1 sample is more intensive than that of the A4 sample, some corrosion signs exist on the transfer film. Additionally, there are more plows on the wear track of A1.

Generally, modulation periods, number and composition of the interface, Ag nanoparticles, surface roughness, hardness, etc. can influence the tribological properties of the multilayer film. The multilayer design can inhibit crack propagation at the interface due to the energy dissipation and make ions in solution encounter a more tortuous path in traversing the film.[31,32] The surface roughness can affect the real contact area of counterpart, and thus the vertical force on the aspires, and then the friction behavior of the film. However, when tested in solution, it has little effect on the frictional behavior of the film, especially for the film with little difference in surface roughness.

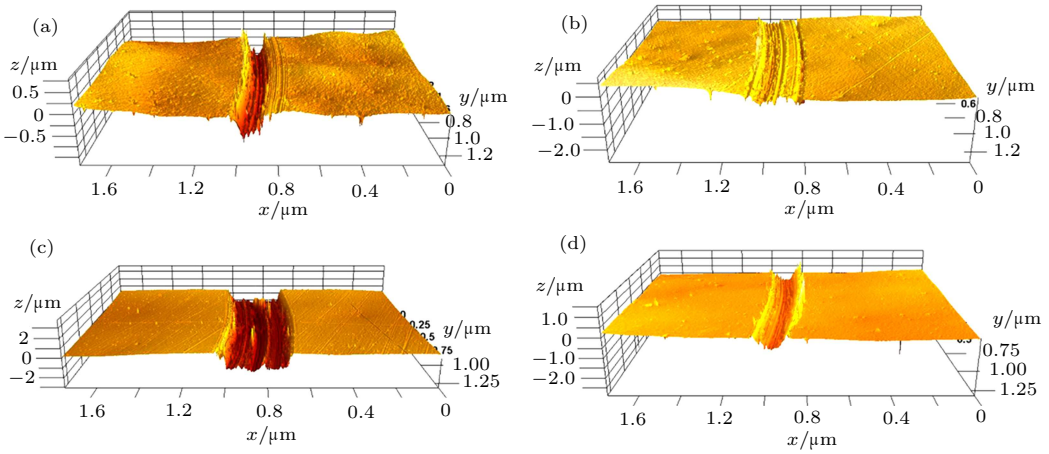


Fig. 10. The 3D optical profile images of worn track on film.

Combining the chemical composition of the transfer film on the Al_2O_3 ball (Table 3), it can be seen that there are no Si nanoparticles in the transfer films except the A3 sample film. Although Si nanoparticles play an important role in the solution friction and wear, Ag nanoparticles and hardness seem to play a more important role in the friction and wear behavior of the multilayer film. As reported before, when nanoparticles were used as friction modifiers, they displayed four behaviors:[33] rolling of nanospheres,[34] tribofilm formation as a result of tribochemical reactions,[35] mending effect

because of the minimal size,[36] and polishing.[37] Especially, the soft Ag nanoparticles on the counterface can possess low shearing stress and avoid severe failure. Furthermore, the appropriate size of Ag allows them to easily enter into the contact interface for load bearing and lubricating. High surface-to-volume ratio enables them to react with their environment. The nanoparticles will undergo sliding and rolling process, and thus the low friction and wear (as shown in Fig. 12).[38]

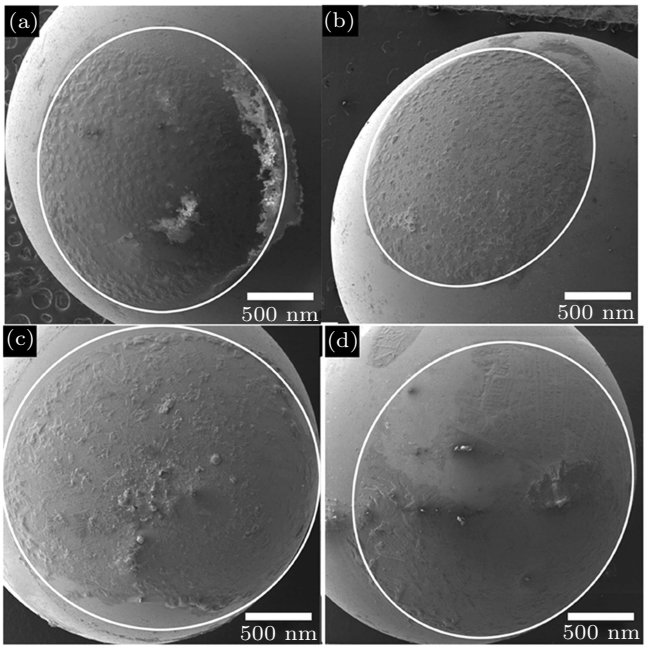


Fig. 11. SEM images of the corresponding Al_2O_3 ball surfaces.

Table 3. Chemical compositions of transfer film on Al_2O_3 ball.

Sample	Chemical composition/at.%			
	C	Si	O	Na + Cl + Mg + Ca + Al
A1	53.39	0.00	20.90	25.72
A2	44.80	0.00	23.25	31.96
A3	51.44	2.58	22.16	28.85
A4	68.07	0.00	15.24	16.68

Notably, compared with the Si/a-C: H multilayer film, the Si/a-C:H(Ag) multilayer films can reduce the sensitivity, friction and wear in salt solution.[6] Furthermore, the film with appropriate Ag content (such as A1 and A4 films) maintains relatively high hardness and thus can provide low friction and wear during the test. For the A1 sample, the a-C:H (Ag) sublayer is the thickest, and the highest sp^2 C content and Ag nanoparticles in the surface sublayer reduce the connectivity and rigidity of the carbon network, and thus increasing the corrosion and wear. When the a-C:H (Ag) sublayer is worn out, the SiC interface and Si sublayer can provide a much steady and less wear. Therefore, the friction coefficient is fluctuant and high at first, and then becomes lower and steadier. The A3 sample with low hardness cannot afford high bearing capacity and thus high friction and wear. Summarily, the incorporating of adequate Ag nano-crystallites into a-C:H sublayer can improve the mechanical and tribological properties of the multilayer film.

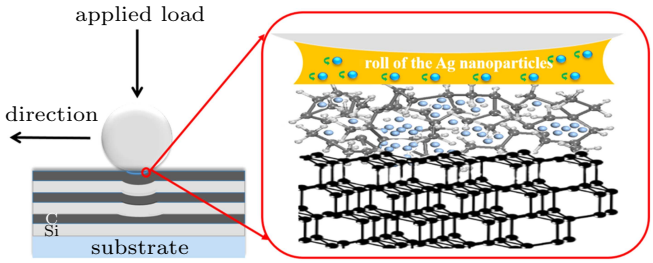


Fig. 12. Schematic illustration of tribological mechanism of A2 sample in stimulated body fluid.

4. Conclusions and perspectives

The Si/a-C:H(Ag) multilayer films with different modulation periods are deposited on stainless steel and silicon substrate by magnetron sputtering and their composition, microstructure, mechanical and tribological properties are examined. Incorporating Ag into the a-C:H sublayer is to improve the film properties, and it proves to play an important role in the properties of the multilayer film. In this study, with the modulation period decreasing from 984 nm to 250 nm, the concentration of C atoms first increases and then decreases. While the concentration of Ag atoms shows an opposite variation trend. Each sublayer in the film is combined well by the SiC formation on the interface. However, the a-C:H sublayer of the film with an appropriate Ag atom concentration (8.97 at.%) (modulation period of 512 nm) maintains the highest sp^3/sp^2 ratio, surface roughness and hardness, and excellent tribological properties in the stimulated body fluid. An appropriate number and size of Ag nanoparticles allow them to easily enter into the contact interface for load bearing and lubricating. High surface-to-volume ratio enables them to react with their environment, and thereby provoding a low friction and wear.

References

[1] Delplancke-Ogletree M and Monteiro O R 1998 *Surf. Coatings Technol.* **108** 484
[2] Lu X C, Luo J B and Zhang Z Y 2007 *Chin. Phys.* **16** 3790
[3] Zhang W, Tanaka A, Xu B S and Koga Y 2005 *Diamond and Related Materials* **14** 1361
[4] Cui J, Qiang L, Zhang B, Ling X, Yang T and Zhang J 2012 *Appl. Surf. Sci.* **258** 5025
[5] Qiang L, Zhang B, Zhou Y and Zhang J 2013 *Solid State Sci.* **20** 17
[6] Baba K, Hatada R, Flege S, Ensinger W, Shibata Y, Nakashima J, Sawase T and Morimura T 2013 *Vacuum* **89** 179
[7] Chen S Y, Ou K L, Huang W C, Chu K T and Ou S F 2013 *Ceramic International* **39** 2575
[8] Yaremchuk I, Meskinis S, Fitio V, Bobitski Y, Slapikas K, Ciegis A, Balevicius Z, Selskis A and Tamulevicius S 2015 *Nanoscale Res. Lett.* **157** 7
[9] Bao K, Ma S L, Xu C H and Cui T 2017 *Acta Phys. Sin.* **66** 036102 (in Chinese)

[10] Velasco S C, Cavaleiro A and Carvalho S 2016 *Prog. Mater. Sci.* **84** 158

[11] Linan Z, Yanxia W, Shujiao Z, Shengwang Y, Bin T, Ying L, Bing Z and Yanyan S 2018 *J. Phys. D: Appl. Phys.* **51** 035302

[12] Li T T, Yang T, Fang J, Zhang D K, Sun J, Wei C C, Xu S Z, Wang G C, Liu C C, Zhao Y and Zhang X D 2016 *Chin. Phys. B* **25** 046101

[13] Wang J, Li S, Zhao Y, Shi J, Lv L, Wang H, Zhang Z and Feng W 2018 *RSC Adv.* **8** 6660

[14] Nakazawa H, Magara K, Takami T, Ogasawara H, Enta Y and Suzuki Y 2017 *Thin Solid Films* **636** 177

[15] Jana S, Das S, De D, Mondal A and Gangopadhyay U 2018 *Mater. Res. Express* **5** 025601

[16] Guo C Q, Pei Z L, Fan D, Gong J and Sun C 2015 *Diamond and Related Materials* **60** 66

[17] Li J, He X, Hang R, Huang X, Zhang X and Tang B 2017 *Ceramic International* **43** 13683

[18] Chandraá Mathpal M, KumaráTripathi A and KumaráSingh M 2015 *RSC Adv.* **5** 12555

[19] Manoj B and Kunjomana A 2012 *Int. J. Electrochem. Sci.* **7** 3127

[20] Ji L, Wu Y, Li H, Song H, Liu X, Ye Y, Chen J, Zhou H and Liu L 2015 *Vacuum* **115** 23

[21] Radić N, Pivac B, Meinardi F and Koch T 2005 *Mater. Sci. Eng. A* **396** 290

[22] Irmer G and Dorner-Reisel A 2005 *Adv. Eng. Mater.* **7** 694

[23] Okubo H and Sasaki S 2017 *Tribology International* **113** 399

[24] Buşilă M, Muşat V, Textor T and Mahltig B 2015 *RSC Adv.* **5** 21562

[25] Mohsen Soltani E, Ghorannevis Z and Shirazi M 2013 *Adv. Mater. Sci. Eng.* 15

[26] Wu Y, Chen J, Li H, Ji L, Ye Y and Zhou H 2013 *Appl. Surf. Sci.* **284** 165

[27] Tavares C, Rebouta L, Alves E, Almeida B, Sousa J B, Da Silva M and Soares J 1998 *Nucl. Instrum. Methods Phys. Res. B* **136** 278

[28] Xu Z, Sun H, Leng Y X, Li X, Yang W and Huang N 2015 *Appl. Surf. Sci.* **328** 319

[29] Wang Y, Li H, Ji L, Liu X, Wu Y, Lv Y, Fu Y, Zhou H and Chen J 2012 *J. Phys. D: Appl. Phys.* **45** 295301

[30] Cruz R, Rao J, Rose T, Lawson K and Nicholls J 2006 *Diamond and Related Materials* **15** 2055

[31] Cui M, Pu J, Zhang G, Wang L and Xue Q 2016 *RSC Adv.* **6** 28570

[32] Holleck H and Schier 1995 *Surf. Coatings Technol.* **76** 328

[33] Tang Z and Li S 2014 *Current Opinion in Solid State and Materials Science* **18** 119

[34] Wu Y, Tsui W and Liu T 2007 *Wear* **262** 819

[35] Zhou J, Yang J, Zhang Z, Liu W and Xue Q 1999 *Mater. Res. Bull.* **34** 1361

[36] Liu G, Li X, Qin B, Xing D, Guo Y and Fan R 2004 *Tribology Letters* **17** 961

[37] Tao X, Jiazheng Z and Kang X 1996 *J. Phys. D: Appl. Phys.* **29** 2932

[38] Dai W, Kheireddin B, Gao H and Liang H 2016 *Tribology International* **102** 88